

## Interplay of flat electronic bands with Holstein phonons

Chunhan Feng \* and Richard T. Scalettar 

Department of Physics, University of California, Davis, California 95616, USA



(Received 19 September 2020; accepted 10 December 2020; published 23 December 2020)

Existing quantum Monte Carlo studies have investigated the properties of fermions on a Lieb ( $\text{CuO}_2$ ) lattice interacting with on-site or near-neighbor electron-electron coupling. Attention has focused on the interplay of such interactions with the macroscopic degeneracy of local zero-energy modes, from which Bloch states can be formed to produce a flat band in which energy is independent of momentum. The resulting high density of states, in combination with the Stoner criterion, suggests that there should be pronounced instabilities to ordered phases. Indeed, a theorem by Lieb rigorously establishes the existence of ferrimagnetic order. Here we study the charge density wave phases induced by electron-phonon coupling on the Lieb lattice, as opposed to previous work on electron-electron interactions. Our key result is the demonstration of charge density wave phases at one third and two thirds fillings, characterized by long-range density-density correlations between doubly occupied sites on the minority or majority sublattices, and an accompanying gap. We also compute the transition temperature to the ordered phase as a function of the electron-phonon coupling.

DOI: [10.1103/PhysRevB.102.235152](https://doi.org/10.1103/PhysRevB.102.235152)

### I. INTRODUCTION

A number of periodic tight-binding lattices contain a macroscopic degeneracy of local, zero-energy eigenstates which arise from the perfect cancellation of hopping for an appropriately phased occupation state [1,2]. These include the kagome, sawtooth, Creutz, diamond-octagon, square-octagon, and decorated honeycomb lattices and, finally, the dice lattice, where the phenomenon was first noted [3]. One of the most prominent examples is the Lieb lattice, shown in Fig. 1, which is of special interest as the structure of the  $\text{CuO}_2$  planes of the cuprate superconductors.

The existence of these “compact localized states” is a property of the noninteracting system. Several years after their discovery, it was pointed out that precise statements can be made concerning the role of repulsive electron-electron interactions in flat-band systems. Specifically, the existence of a ferrimagnetic ground state can be rigorously established [4]. Subsequent work further investigated flat-band ferromagnetism [5–8]. The effect of attractive electron-electron interactions is also of interest [9–12], especially since the momentum at which Bose-Einstein condensation of fermionic pairs might occur is uncertain in a flat band [13–15].

Flat bands have also been considered within the context of the fractional quantum Hall effect [16], Chern insulating behavior [17], Tomonaga-Luttinger liquids [18], and Haldane phases [19]. Perhaps the most dramatic explosion of theoretical and computational interest coincided with the recent discovery that bilayer graphene, when twisted at a “magic angle” of about  $1.1^\circ$ , displays unconventional superconductivity (SC), which is likely closely linked to the appearance of a nearly dispersionless bands in the effective moiré pattern

lattice [20–25]. This SC is characterized by a ratio of critical temperature to Fermi temperature higher than the cuprates.

In addition to realizations in these solid-state materials, flat-band physics has also been explored in photonic Lieb lattices [26,27] and optical Lieb [28,29], kagome [30], and honeycomb [31] lattices.

Here we investigate the phases of interacting *electron-phonon* systems for flat electronic bands [32]. Specifically, we study the Holstein Hamiltonian on a Lieb lattice. Although there are suggestive analogies between the Holstein model and the attractive Hubbard model, the former has a nontrivial frequency-dependent coupling which distinguishes the two situations, the most significant consequence of which is the presence of a finite-temperature phase transition even on two-dimensional (2D) lattices, which are the most commonly investigated flat-band geometries. It is only in the extreme antiadiabatic limit, where the phonon frequency is one to two orders of magnitude larger than the electronic bandwidth, that the Holstein and attractive Hubbard models become quantitatively equivalent [33].

The structure of this paper is as follows: After introducing the model (Sec. II) and computational methodologies (Sec. III), we show the behavior of the compressibility, double occupancy, spectral function, and charge density wave structure factor (Sec. IV). Together these observables point to the formation of a gapped charge density wave (CDW) state below a critical temperature  $T_c$ , whose value we determine using finite-size scaling. The final section summarizes our findings.

### II. HOLSTEIN MODEL

The Holstein model [34] we consider consists of a collection of electrons, described by fermionic creation and destruction operators  $\hat{d}_{i\sigma}^\dagger$ ,  $\hat{d}_{i\sigma}$  hopping between near-neighbor

\*chhfeng@ucdavis.edu

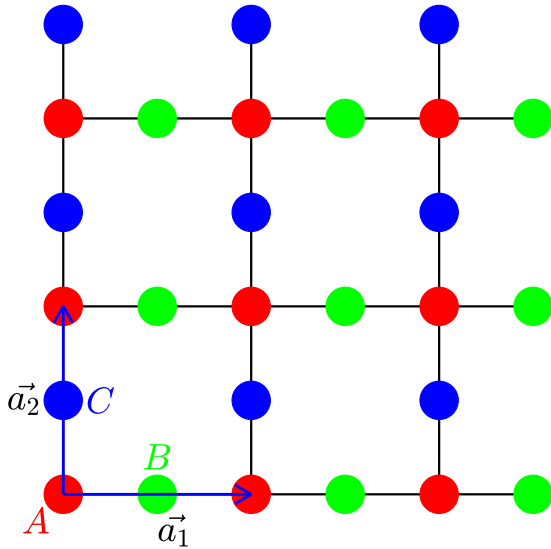


FIG. 1. The Lieb lattice geometry. Additional sites (blue and green) are added to the midpoint of each of the bonds linking the sites of a square lattice (red). The resulting structure is bipartite and has three sites per unit cell. Note especially that the red sublattice contains only half as many sites as the sublattice comprising blue and green sites. The blue-green pattern of sites surrounding one of the vacancies illustrates a zero-energy mode. See the text for more details.

sites on the Lieb lattice shown in Fig. 1. The electron density on each site,  $\hat{n}_i = \hat{n}_{i\uparrow} + \hat{n}_{i\downarrow}$ , with  $\hat{n}_{i\sigma} = \hat{d}_{i\sigma}^\dagger \hat{d}_{i\sigma}$ , where  $i$  denotes lattice sites and  $\sigma$  is the spin index, couples linearly to the displacement  $\hat{x}_i$  of a local quantum oscillator degree of freedom. The Hamiltonian is therefore

$$\begin{aligned} \mathcal{H} = & -t \sum_{(i,j),\sigma} (\hat{d}_{i\sigma}^\dagger \hat{d}_{j\sigma} + \text{H.c.}) - \mu \sum_{i,\sigma} \hat{n}_{i\sigma} \\ & + \frac{1}{2} \sum_i (\hat{p}_i^2 + \omega_0^2 \hat{x}_i^2) + \lambda \sum_{i,\sigma} \hat{x}_i \hat{n}_{i\sigma}. \end{aligned} \quad (1)$$

We have set the oscillator mass  $M = 1$  and will also use units in which  $\hbar = k_B = 1$  and the hopping amplitude  $t = 1$ . The chemical  $\mu = -\lambda^2/\omega_0^2$  corresponds to half filling.

The Lieb lattice Hamiltonian is sometimes studied with an additional ‘‘charge transfer’’ term in the form of an energy difference between the sites on the two sublattices. We do not include such a term here. Its inclusion would favor one of the two degenerate CDW phases and preempt the spontaneous symmetry-breaking phase transition which is our focus here.

The electronic density of states in the absence of the electron-phonon interactions is given in Fig. 2. The  $\delta$ -function spike at  $E = 0$  reflects the macroscopic degenerate collection of local  $E = 0$  vectors  $|\psi\rangle$  constructed by forming a state with equal amplitude and opposite phases on the four blue and green sites surrounding any vacant site on the Lieb lattice (see Fig. 1). All these  $|\psi\rangle$  have the property  $\hat{\mathcal{K}}|\psi\rangle = 0$ , where  $\hat{\mathcal{K}}$  is the first (hopping) term in Eq. (1). The band structure is given in Fig. 3

When  $\lambda \neq 0$ , the qualitative physics of the Holstein model is as follows: At low densities individual electrons distort the lattice sites in their vicinity. The resulting composite particle,

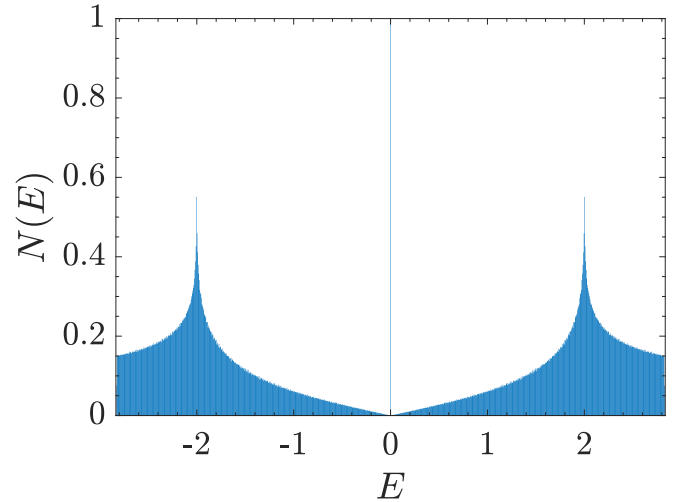


FIG. 2. The density of states of the Lieb lattice. Energy levels of two dispersing bands bracket the  $\delta$ -function peak at  $E = 0$ . Particle-hole symmetry is reflected in the property  $N(E) = N(-E)$ .

a ‘‘polaron,’’ possesses an increased effective mass, reflecting the fact that when the electron hops between sites, the oscillator degrees of freedom must reconfigure themselves [35–39]. These dressed quasiparticles tend to attract one another since the distortion caused by one provides a favorable environment for another. Indeed, solving the  $t = 0$  Holstein model, one can see an effective attraction  $U_{\text{eff}} = -\lambda^2/\omega_0^2$  exists between spin-up and -down fermions. This independent site form is consistent with the interaction between electrons mediated by a phonon propagator,  $V_{\text{eff}}(\omega) = \lambda^2/(\omega^2 - \omega_0^2)$ , if one sets  $\omega = 0$ .

The pairs of up and down electrons which arise from this attraction can participate in ordered phases. One possibility, which dominates on half-filled ( $n_{i,\sigma} = 1/2$ ) bipartite lattices with equal numbers of sites in the two sublattices, such as square and honeycomb geometries, is a CDW arrangement in which pairs occupy one of the two sublattices. CDW formation is energetically favorable because, by surrounding itself

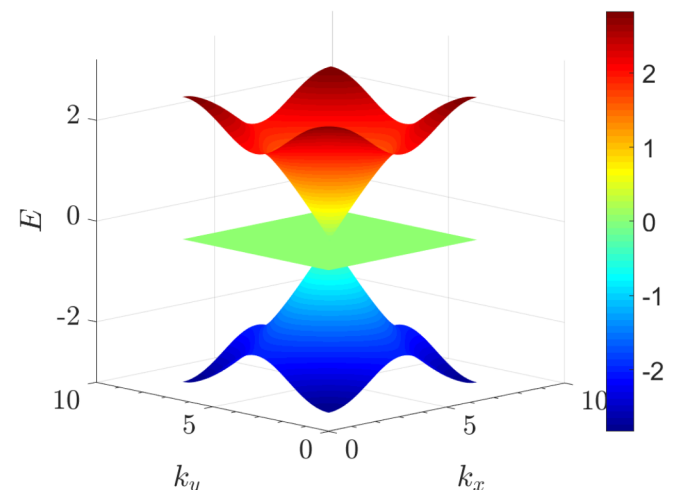


FIG. 3. The band structure of the Lieb lattice.

with empty sites, a pair of electrons has the optimal ability for virtual hopping processes to adjacent sites, thereby lowering its energy by  $J \sim -zt^2/U_{\text{eff}}$ , where  $z$  is the coordination number. This situation is similar to that giving rise to antiferromagnetic order in the half-filled repulsive Hubbard model.

Another possible ordered state occurs when the pairs condense into a superconducting phase. This is expected to occur when the system is doped away from fillings which favor CDW order and has been studied with, for example, Eliashberg theory [40–45]. Quantum Monte Carlo (QMC) simulations have given indications of pairing as well [46–48].

In this paper, we consider the CDW transition in the Holstein model on the Lieb lattice. We set the phonon frequency  $\omega_0/t = 1$  to facilitate comparisons with most of the existing QMC literature [46,47,49–56]. This historical choice was, in part, made as a simple starting point to explore the qualitative physics of the CDW and SC transitions but also because it facilitated the determinant quantum Monte Carlo (DQMC) simulations, which are known to exhibit long autocorrelation times at  $\omega_0/t \lesssim 1/2$ . Recent algorithmic improvements have made possible the study of smaller  $\omega_0$  [57–61].

### III. COMPUTATIONAL METHODOLOGIES

#### A. Mean-field theory

We use the adiabatic approximation, ignoring the  $\hat{p}_i^2$  term, and assume a staggered pattern of phonon displacements with the ansatz  $x_i = x_0 - \Delta$  for sublattice A and  $x_i = x_0 + \Delta$  for sublattice B/C. Inserting this ansatz into Eq. (1), the resulting quadratic fermion Hamiltonian can be diagonalized. Then the free energy is a function of  $x_0$ ,  $\Delta$ , and inverse temperature  $\beta$ ,

$$F = \frac{1}{2}N\omega_0^2(x_0^2 + \Delta^2 + \frac{2}{3}Nx_0\Delta) - \frac{1}{\beta} \sum_{\alpha,\sigma,\mathbf{k}} \ln(1 + e^{-\beta\epsilon_\alpha}), \quad (2)$$

where

$$\epsilon_\alpha = \begin{cases} \lambda\Delta + \lambda x_0 - \mu, \\ \pm \sqrt{(\lambda\Delta)^2 + 4t^2(\cos^2 \frac{k_x}{2} + \cos^2 \frac{k_y}{2})} + \lambda x_0 - \mu \end{cases}$$

are the three fermion energy bands and  $\mathbf{k} = (k_x, k_y)$  are allowed momentum vectors. At a fixed temperature  $T$ , we determine the  $(x_0^*, \Delta^*)$  which minimize  $F$ . Results obtained by this approach will be presented in the next section.

#### B. Determinant quantum Monte Carlo

Although much insight can be gleaned from mean-field theory (MFT), especially concerning the possible types of order, it has a number of well-understood defects, especially an overestimate of the tendency to long-range order arising from ignoring fluctuations. This is particularly evident in lattice models like the Hubbard and Holstein Hamiltonians, where it fails to distinguish two separate energy scales. The first is the temperature  $T \sim U$  at which local moments (in the case of repulsive interactions) or pairs (in the case of attractive interactions) form. The second is the temperature at which intersite ordering occurs. Since the former grows linearly with the interaction strength  $U$  and the latter falls as  $1/U$ , MFT overestimates  $T_c$  by a far wider margin at strong coupling than

in simpler classical descriptions of long-range order such as the Ising model.

To provide a more accurate treatment of the electron-phonon correlations, we turn to the use of the DQMC methodology [62,63]. In this approach, the full imaginary time propagator  $e^{-\beta\hat{H}}$  is written as a product of incremental factors  $e^{-\Delta\tau\hat{H}}$ . This discretization allows for the ‘‘Trotter’’ approximation,  $e^{-\Delta\tau\hat{H}} \approx e^{-\Delta\tau\hat{H}_1}e^{-\Delta\tau\hat{H}_2}$ , with  $\hat{H} = \hat{H}_1 + \hat{H}_2$ . The purpose of dividing up the imaginary-time evolution is that the matrix elements of the individual pieces can be evaluated analytically. In particular, upon the introduction of complete sets of phonon states, the fermionic trace in the resulting quadratic form of fermionic operators can be performed, leaving a trace over a phonon field  $x(\mathbf{i}, \tau)$  which depends on both spatial site  $\mathbf{i}$  and imaginary time slice  $\tau$ . The integrand has both a bosonic piece from the quantum oscillator term in  $\hat{H}$  and a product of two determinants (one from each spin species) which depend on  $x(\mathbf{i}, \tau)$ . For the Holstein model, because the up and down species couple to the phonon coordinate in the same way, the determinants are identical. The fermion sign problem is absent in the resulting square of determinants.  $x(\mathbf{i}, \tau)$  is sampled stochastically.

DQMC treats interacting quantum Hamiltonians exactly. The sole (controlled) approximation is in the discretization of  $\beta$ . With the usual choices of  $\Delta\tau$  the associated errors are easily made smaller than those arising from the sampling. (The exception is for local quantities like the energy and double occupancy whose statistical errors are extremely small. For these observables, a  $\Delta\tau \rightarrow 0$  extrapolation is straightforward to perform.) Simulations are carried out on lattices of finite size, necessitating a finite-size scaling analysis, as described below.

We focus on several local observables, the density  $\rho = \langle \hat{n}_i \rangle$  and double occupancy  $\mathcal{D} = \langle \hat{n}_{i\uparrow}\hat{n}_{i\downarrow} \rangle$ , and on the CDW structure factor, the Fourier transform of the real-space density-density correlation function.

$$S(\mathbf{q}) = \sum_{\mathbf{r}} c(\mathbf{r}) e^{i\mathbf{q}\cdot\mathbf{r}}, \quad (3)$$

$$c(\mathbf{r}) = \langle \Delta\hat{n}_{i+\mathbf{r}} \Delta\hat{n}_i \rangle$$

where  $\Delta\hat{n}_i = \sum_{\sigma} \Delta\hat{n}_{i,\sigma} = \sum_{\sigma} \hat{n}_{iB,\sigma} + \hat{n}_{iC,\sigma} - 2\hat{n}_{iA,\sigma}$  is the charge density difference within a unit cell, labeled by  $\mathbf{i}$ . When only the A or B/C sublattice is occupied, corresponding to one third or two thirds filling, the dominant  $S(\mathbf{q})$  will be  $S_{\text{cdw}} = S(0, 0)$ .

The spectral function  $A(r, \omega)$  is obtained by an analytic continuation of the nonequal-time Green’s function

$$G(\mathbf{r}, \tau) = \langle \hat{c}_{i+\mathbf{r},\sigma}(\tau)\hat{c}_{i,\sigma}(0) \rangle$$

$$= \langle e^{\tau\hat{H}}\hat{c}_{i+\mathbf{r},\sigma}(0)e^{-\tau\hat{H}}\hat{c}_{i,\sigma}(0) \rangle,$$

$$G(\mathbf{r}, \tau) = \int d\omega A(\mathbf{r}, \omega) \frac{e^{-\omega\tau}}{e^{\beta\omega} + 1}. \quad (4)$$

We report the Fourier transform of the spectral function at zero distance, a quantity which is the analog of the noninteracting density of states in a correlated system.

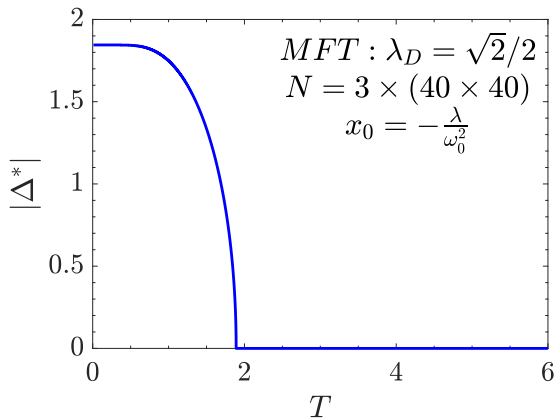


FIG. 4. Mean-field order parameter  $\Delta^*$  as a function of temperature  $T/t$  at half filling,  $\mu = -\frac{\lambda^2}{\omega_0^2} = -4$ . Here and in all subsequent figures  $\omega_0/t = 1$ . For  $T > T_c \sim 1.9t$ , the MFT critical temperature  $\Delta^* = 0$ , and each site has  $\rho_i = 1/2$  per spin. For  $T < T_c$  there are two degenerate values of  $\Delta = \pm\Delta^*$  which minimize  $\mathcal{F}$ . These correspond to  $1/2 - d\rho$  and  $1/2 + d\rho$  (and hence the *average* density is half filled). (See Fig. 5 and the text for more discussion.)

DQMC has been used to explore various properties of the attractive and repulsive Hubbard models on the Lieb lattice [15,64,65] but has not yet been used for the Holstein model.

## IV. RESULTS

### A. Mean-field theory

We first explore the effect of electron-phonon interaction by using the mean-field theory approach described in Sec. III A. Since the  $\lambda x_i n_i$  term in the mean-field Holstein Hamiltonian can be viewed as a chemical potential  $\lambda x_i$  acting on site  $\mathbf{i}$ , a nonzero bond dimerization  $\Delta$  implies a staggered pattern of electron density, i.e., a CDW phase. We set  $\mu = -\frac{\lambda^2}{\omega_0^2}$  so that the lattice is half filled. The corresponding  $x_0 = -\frac{\lambda}{\omega_0^2}$ .

The value  $\Delta^*$  which minimizes  $\mathcal{F}$  is plotted as a function of temperature  $T$  in Fig. 4. For  $T > T_c \sim 1.9t$ , the order parameter  $\Delta^* = 0$ , and there are equal sublattice densities  $\rho_A = \rho_{B/C} = 1/2$  per spin (see also Fig. 5). Below  $T_c$ , we find there is a degenerate pair of nonzero solutions  $\pm\Delta^*$  and distinct densities  $\rho_A; \rho_{B/C}$  on the two sublattices. We denote the densities per spin on the *whole* lattice, i.e., averaged over sublattices,  $(\rho_A + 2\rho_{B/C})/3$ , by  $1/2 \pm d\rho$ . The two signs are associated with the two signs  $\pm\Delta^*$ . A change in sign of  $\Delta^*$  can be viewed as an interchange  $A \leftrightarrow B/C$  of the high- and low-occupation sublattices. Since the numbers of sites in the two sublattices are unequal, this also shifts the density on the whole lattice (unlike the more conventional cases of square and honeycomb bipartite lattices).

Perfect CDW order, in which  $1/2 \pm d\rho = 1/3, 2/3$  and  $(\rho_A; \rho_{B/C}) = (1, 0)$  or  $(0, 1)$ , requires the absence of both thermal ( $T \rightarrow 0$ ) and quantum ( $\lambda^2/\omega_0^2 \rightarrow \infty$ ) fluctuations. In Fig. 4,  $\Delta^*$  increases to a maximal value  $\Delta^* \sim 1.85$  at zero temperature.  $\Delta^* = 2$  would yield a perfect CDW pattern. That  $\Delta^* < 2$  reflects the presence of some residual quantum fluctuations:  $\lambda^2/\omega_0^2$  is finite. Not surprisingly, in Fig. 5, the

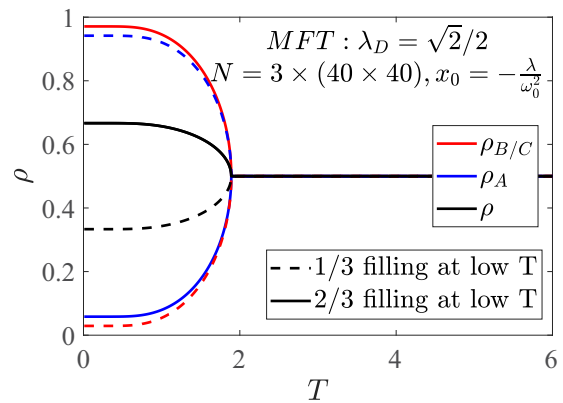


FIG. 5. Black solid ( $-\Delta^*$ ) and dashed ( $+\Delta^*$ ) curves denote the electron density per spin on the whole lattice,  $\rho$ . Blue and red give densities on the two sublattices  $\rho_A$  and  $\rho_{B/C}$ . The horizontal axis is temperature  $T$ . For  $T > T_c \sim 1.9t$ , the MFT critical temperature, each sublattice has  $\rho_A = \rho_{B/C} = 1/2$  per spin. For  $T < T_c$ , there are two degenerate states. The densities bifurcate into two curves associated with the pair of degenerate values  $\pm\Delta^*$  of the order parameter.

density per spin  $\rho_{B/C}$  (red) is closer to the perfect CDW state,  $\rho = 0$  (empty) or  $\rho = 1$  (doubly occupied), than the density  $\rho_A$  (blue). This is because sites A have twice as many nearest neighbors as sites B/C. The larger number of hoppings  $t$  produce more quantum fluctuations.

All MFT results presented in this paper are obtained on a  $3 \times (40 \times 40)$  Lieb lattice with a dimensionless electron phonon coupling constant  $\lambda_D \equiv \frac{\lambda^2}{\omega_0^2 W} = \sqrt{2}/2$ . Here  $W = 4\sqrt{2}t$  is the fermion bandwidth for a Lieb lattice in the noninteracting limit. We will see later the MFT  $T_c \sim 1.9t$  is more than an order of magnitude higher than  $T_c$  given by DQMC.

For different chemical potentials  $\mu$ , we follow the same steps to determine  $(x_0^*, \Delta^*)$  minimizing the free energy and find  $\Delta^* > 0$  ( $\rho = 1/3$  CDW pattern) when  $\mu < -\frac{\lambda^2}{\omega_0^2}$ ;  $\Delta^* < 0$  ( $\rho = 2/3$  CDW pattern) when  $\mu > -\frac{\lambda^2}{\omega_0^2}$ . The electron density can be obtained by  $n = \sum_{\alpha, \mathbf{k}} \frac{1}{1 + e^{\beta \epsilon_{\alpha}}}$ . Figure 6 shows the density  $\rho$  per spin as a function of chemical potential  $\mu$ . As temperature is lowered, plateaus at  $\rho = 1/3$  and  $\rho = 2/3$  develop, indicating that a  $1/3$  filling CDW pattern and its partner at  $2/3$  filling extend over a finite range of  $\mu$ , which is consistent with the DQMC results below. A similar phenomenon is also observed in the “ $t$ - $V$  model” of spinless fermions interacting with a nearest-neighbor repulsion on a Lieb lattice [66].

### B. Determinant quantum Monte Carlo

We now turn to DQMC results. We begin with the spectral function in Fig. 7. At high temperatures (small  $\beta$ )  $A(\omega = 0)$  is nonzero. A gap is fully formed at  $\beta_c t \sim 6$ , suggesting a transition to an insulating CDW phase.

A more accurate determination of the location of the CDW transition is obtained by a finite-size scaling analysis of  $S_{\text{cdw}}$ . Because the low-temperature phase involves occupying one of two spatial sublattices, it breaks  $\mathcal{Z}_2$  symmetry, and therefore, the transition should be in the Ising universality class. Using

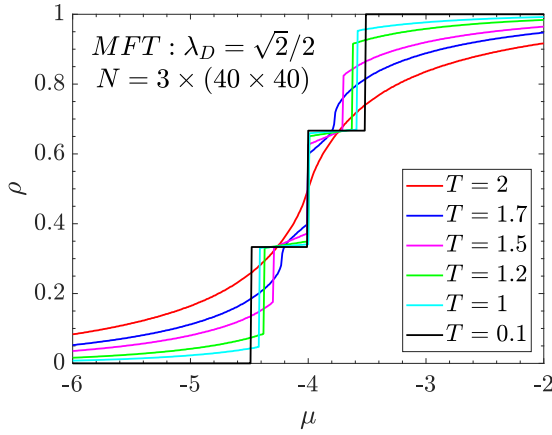


FIG. 6. Density per spin  $\rho$  as a function of chemical potential  $\mu$  within MFT. Temperature  $T = 2t > T_c$ , and  $\rho(\mu)$  is smooth. For temperature  $T = t < T_c$  the density  $\rho(\mu)$  (per spin) has plateaus at  $\rho = 1/3, 2/3$  corresponding to a nonzero CDW gap. The sublattice spin occupations are shown in Fig. 5. When  $\Delta^* > 0$ , there are a smaller number of A sites with  $\rho > 1/2$  and a larger number of B/C sites with  $\rho < 1/2$ , and the total density  $\rho \sim 1/3$  (see text) and vice versa for  $\Delta^* < 0$ .

the known 2D Ising critical exponents  $\nu = 1$  and  $\gamma/\nu = 7/4$  yields the finite-size scaling plots of Fig. 8. We find  $\beta_c t = 6.4 \pm 0.1$ . If we eschew this knowledge and instead vary the critical exponents and minimize the scatter of the data collapse plot, the resulting  $\gamma/\nu$  is within 5% of the 2D Ising value. An example of such an analysis (for the honeycomb lattice) is given in [53].

The real-space density correlations  $c(\mathbf{r})$  provide additional insight into the nature of the CDW order. Figures 9 and 10 give color intensity plots of  $c(\mathbf{r})$  for different temperatures and initializations of the phonon displacement  $x(\mathbf{i}, \tau)$ . More specifically, if we start the phonon displacement at  $x_0 - \Delta$  (with  $\Delta > 0$ ), the fermion density on that site tends to be high, while a displacement  $x_0 + \Delta$  is associated with a low density. At high temperatures, the correlations are independent of the starting configuration, and  $c(\mathbf{r}) = \langle n_{i+\mathbf{r}} n_i \rangle = \langle n_{i+\mathbf{r}} \rangle \langle n_i \rangle \sim 1$ .

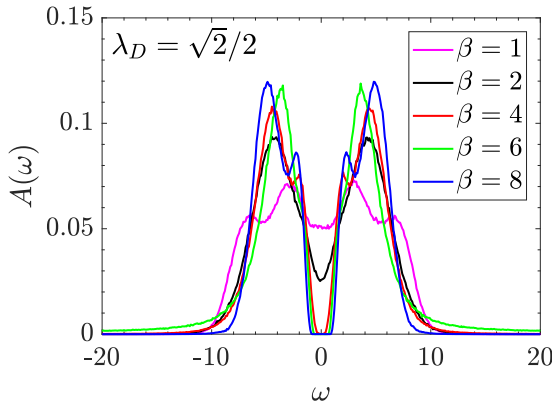


FIG. 7. The spectral function  $A(\omega) = \frac{1}{N} \sum_k A(k, \omega)$  determined in DQMC calculations. A gap opens at the Fermi surface  $\omega = 0$  as the temperature is lowered ( $\beta$  increases). This provides a rough estimate of  $T_c$ .

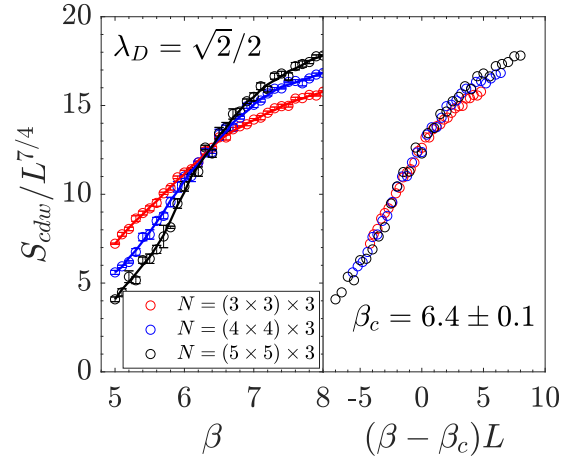


FIG. 8. Left: The scaled structure factor is plotted versus  $\beta$  for three lattice sizes. The crossing gives the position of the CDW transition. Right: If the horizontal (inverse temperature) axis is also scaled, a full data collapse is obtained.

Short-range correlations begin to develop at  $\beta t \sim 6$ , and a strong alternation between  $c(\mathbf{r}) \sim 4$ , where  $\mathbf{r}$  connects a pair of doubly occupied sites, and  $c(\mathbf{r}) \sim 0$ , where one of the sites is empty, becomes apparent. In the case of the initialization in the  $\rho = 1/3$  state (Fig. 9) with only sublattice A sites occupied, density correlations referenced to an A site (top panel) show the alternation, whereas if they are referenced to an unoccupied B site (bottom panel) all  $c(\mathbf{r})$  become small. Conversely, for initialization in the  $\rho = 2/3$  state (Fig. 10) with sublattice B/C sites occupied, density correlations referenced to a B site (bottom panel) show the alternation, whereas if they are referenced to an unoccupied A site (top panel) all  $c(\mathbf{r})$  become small.

Another way to examine the evolution into one of two possible ground states, characterized by distinct densities, is to begin several simulations with constant density  $\rho = 1/2$  per spin and examine the final densities achieved. Figure 11 shows the result for four such simulations. At small  $\beta$  the lattice remains half filled, but as  $\beta$  increases, the lattice falls into either the  $\rho = 1/3$  or  $\rho = 2/3$  minimum. The tendency for this splitting begins about  $\beta \sim 5$ . For  $5 \lesssim \beta \lesssim 9$  the data tend to fill the region between the upper and lower densities. This happens because at finite temperatures and on finite lattices, tunneling between the two minima can occur in the course of a simulation. Depending on the relative amount of time spent at  $\rho = 1/3$  and  $\rho = 2/3$ , the average density can take different values. For  $\beta \gtrsim 9$  very little tunneling occurs, and the data instead lie on just one of the two bounding lines. Note that the order parameter depends on  $\beta$ , so that the increasing width of the  $\rho$  curves reflects the growth of the CDW order parameter below  $\beta_c$ .

It is important to emphasize a subtlety of the physics. Although the simulations in Fig. 11 were done at the chemical potential  $\mu = -\lambda^2/\omega_0^2$ , which should give  $\rho = 1/2$  per spin by particle-hole symmetry, the symmetry is broken, and there are two low-temperature phases with  $\rho = 1/3$  and  $\rho = 2/3$ . This is precisely analogous to a simulation of a magnetic (e.g., Ising) model at zero external field. Although symmetry

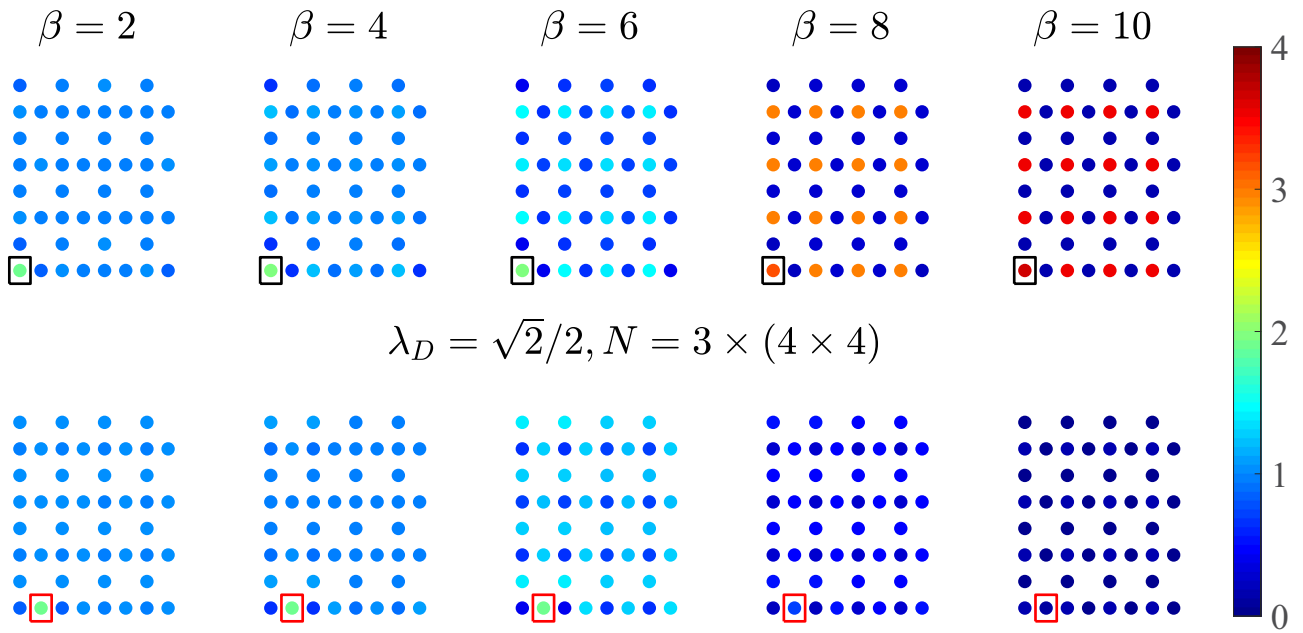


FIG. 9. Density-density correlation for a  $3 \times (4 \times 4)$  Lieb lattice at  $\omega_0 = 1$ ,  $\lambda = 2(\lambda_D = \sqrt{2}/2)$ . The simulation was initialized with a phonon displacement field appropriate to being in the  $\rho = 1/3$  minimum with dominant  $A$  sublattice (“copper sites”) occupation. Top: Correlations between each site and the Cu site in the bottom left unit cell. Bottom: Correlations between each site and the  $B/C$  sublattice (“oxygen sites”) in the bottom left unit cell.

demands magnetization  $M = 0$ , below  $T_c$  there are two phases with  $M = \pm M_*$ .

Plots of the density  $\rho$  versus chemical potential  $\mu$  (Fig. 12) also reveal the CDW phase. At high temperatures  $\rho$  evolves smoothly between the empty and fully packed limits, transiting half filling at the particle-hole symmetry point  $\mu = -\lambda^2/\omega_0^2$ . At temperatures below the CDW transition, a plateau develops in which the compressibility  $\kappa = d\rho/d\mu$  vanishes.

However, unlike the situation on a bipartite lattice in which each sublattice has equal numbers of particles, the plateau is bifurcated by an abrupt jump as the system transitions from occupation of the minority to majority sublattice.

Figure 13 is similar to Fig. 11, except showing the double occupancy  $\mathcal{D}$ . At low  $\beta$  (high  $T$ ),  $\mathcal{D} = \langle n_{i\uparrow} n_{i\downarrow} \rangle \sim \langle n_{i\uparrow} \rangle \langle n_{i\downarrow} \rangle \sim 1/4$ . As  $T$  decreases below the pair binding scale  $U_{\text{eff}} = \lambda^2/\omega_0^2 \sim 4$ , pairs begin to form on half the sites ( $\mathcal{D} \sim$

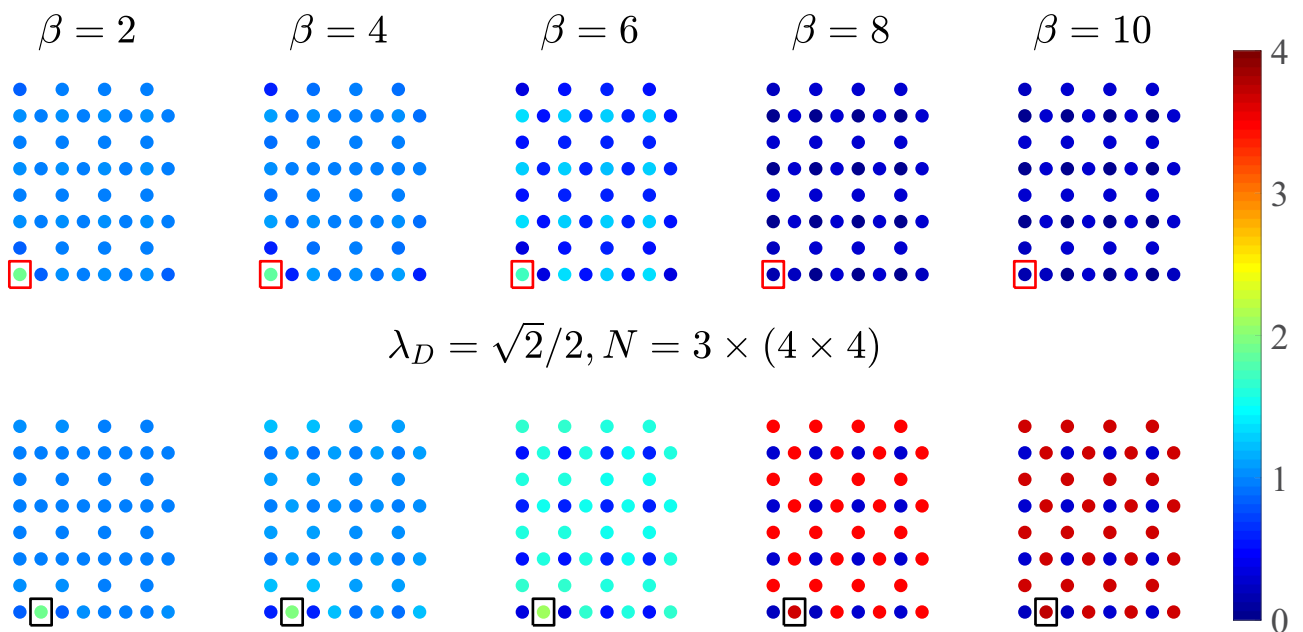


FIG. 10. Same as Fig. 9, except starting in the  $\rho = 2/3$  minimum.

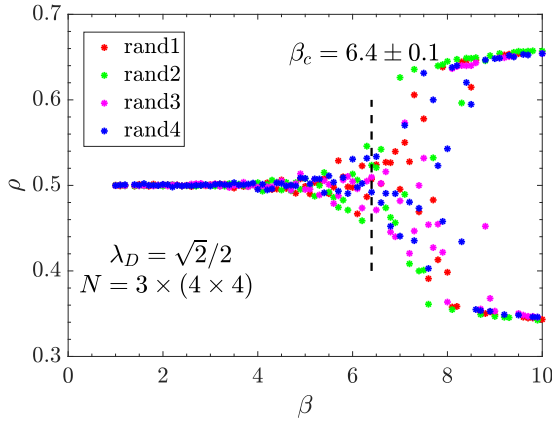


FIG. 11. Density per spin  $\rho$  as a function of  $\beta$  at  $\lambda_D = \sqrt{2}/2$ . Data for four different random seeds are shown. A spontaneous symmetry breaking begins to occur at  $\beta \sim 5$ . See text for details. The vertical dashed line is the value of  $\beta_c$  determined from FSS of  $S_{\text{cdw}}$ .

0.5). At larger  $\beta$  a CDW pattern emerges in which  $D = 0$  or  $D = 1$  depending on which sublattice is occupied.

Figure 14 is the phase diagram of the Holstein model on a Lieb lattice in the plane of temperature-dimensionless coupling constant. We also make a comparison to several other geometries. A striking feature of the plot is that the honeycomb and Lieb lattice values are so close. Naively, one might have argued that the  $\delta$ -function divergence of the Lieb lattice flat-band density of states would lead to a large  $T_c$ , especially when compared to the semimetallic case of the honeycomb lattice. However, the explanation is clear: The Lieb lattice CDW order really occurs for  $\rho = 1/3$  and  $\rho = 2/3$ , where it has Dirac cones much like the honeycomb lattice. Thus, the only difference is that the honeycomb lattice coordination number  $z = 3$ , whereas for the Lieb geometry the average coordination number is slightly smaller,  $\bar{z} = 2/3(2) + 1/3(4) = 8/3$ . Obtaining the weak-coupling behavior of  $T_c$  is a nontrivial analytic calculation. It has been done for the 2D square lattice, yielding good agreement with DQMC simulations similar to those reported here [67].

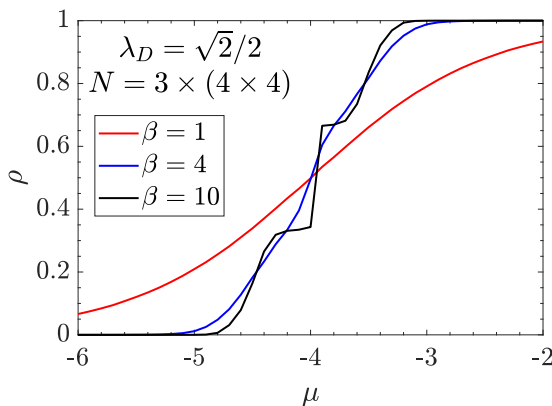


FIG. 12. Density per spin  $\rho$  vs chemical potential  $\mu$  for several different  $\beta$  obtained in DQMC simulations. Here  $\lambda = 2$ , ( $\lambda_D = \sqrt{2}/2$ ).

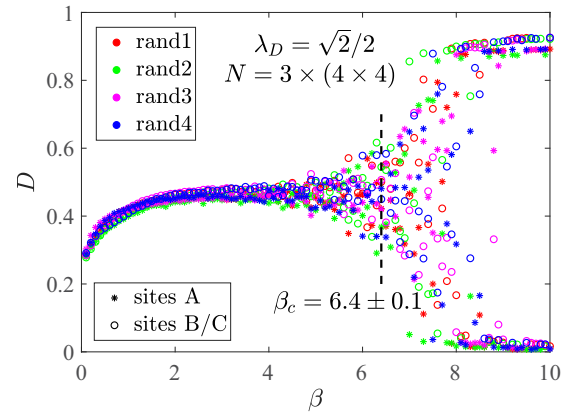


FIG. 13. Double occupancy  $\mathcal{D}$  vs  $\beta$  at  $\lambda = 2(\lambda_D = \sqrt{2}/2)$  for a  $3 \times (4 \times 4)$  lattice and  $\mu = -\lambda^2/\omega_0^2$ . Data for four different random seeds are shown. The vertical dashed line is the value of  $\beta_c$  determined from FSS of  $S_{\text{cdw}}$ . At high  $T$  (small  $\beta$ ), electrons are uncorrelated, and  $D \approx \langle n_{i\uparrow} \rangle \langle n_{i\downarrow} \rangle \sim 0.25$  on every site  $\mathbf{i}$ . As  $T$  decreases, pairs begin to form on half the sites, leaving the other half empty, and the double occupancy increases to  $D \sim 0.5$ . Finally, as  $T$  is further lowered, below  $1/\beta_c$ ,  $1/3$ , and  $2/3$  filling CDW patterns are revealed, with distinct values of  $D$  on the two sublattices, reflecting spontaneous symmetry breaking.

## V. CONCLUSIONS

We have studied the charge density wave transition for the Holstein model on a Lieb lattice. Our interest was in establishing results for the effect of compact localized states (flat bands) on ordered phases driven by the electron-phonon interaction, in analogy with the body of work which exists for electron-electron interactions (primarily the Hubbard model).

The behaviors of the occupation, double occupancy, spectral function, and charge structure factor have been obtained quantitatively and used to infer a phase diagram of critical temperature versus coupling constant.

We emphasize as well that our results for electron-phonon interactions on a Lieb lattice differ from those for electron-electron interactions [15] in a fundamental way. The degeneracy of the superconducting and CDW orders at half

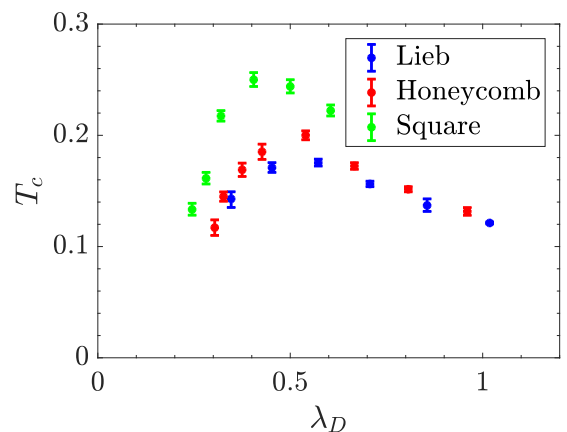


FIG. 14. Critical temperatures for the Lieb lattice (this work) and the honeycomb [53] and square lattices.

filling in the half-filled attractive Hubbard model implies the absence of long-range order except in the ground state (Mermin-Wagner). This symmetry is broken in the Holstein model. As a consequence there is a finite CDW  $T_c$  even on two-dimensional geometries. This is already well known for the square and honeycomb lattices.

## ACKNOWLEDGMENTS

The work of C.F. and R.S. was supported by Grant No. DE-SC0014671 funded by the U.S. Department of Energy, Office of Science.

- 
- [1] O. Derzhko, J. Richter, and M. Maksymenko, Strongly correlated flat-band systems: The route from Heisenberg spins to Hubbard electrons, *Int. J. Mod. Phys. B* **29**, 1530007 (2015).
- [2] D. Leykam, A. Andreanov, and S. Flach, Artificial Flat Band Systems: From Lattice Models to Experiments, *Adv. Phys.: X* **3**, 1473052 (2018).
- [3] B. Sutherland, Localization of electronic wave functions due to local topology, *Phys. Rev. B* **34**, 5208 (1986).
- [4] E. H. Lieb, Two Theorems on the Hubbard Model, *Phys. Rev. Lett.* **62**, 1201 (1989).
- [5] A. Mielke, Ferromagnetic ground states for the Hubbard model on line graphs, *J. Phys. A* **24**, L73 (1991).
- [6] A. Mielke, Ferromagnetism in the Hubbard model on line graphs and further considerations, *J. Phys. A* **24**, 3311 (1991).
- [7] H. Tasaki, Ferromagnetism in the Hubbard Models with Degenerate Single-Electron Ground States, *Phys. Rev. Lett.* **69**, 1608 (1992).
- [8] H. Tasaki, From Nagaoka's Ferromagnetism to Flat-Band Ferromagnetism and Beyond, *Prog. Theor. Phys.* **99**, 489 (1998).
- [9] A. Julku, S. Peotta, T. I. Vanhala, D.-H. Kim, and P. Törmä, Geometric Origin of Superfluidity in the Lieb-Lattice Flat Band, *Phys. Rev. Lett.* **117**, 045303 (2016).
- [10] P. Kumar, T. I. Vanhala, and P. Törmä, Magnetization,  $d$ -wave superconductivity, and non-Fermi-liquid behavior in a crossover from dispersive to flat bands, *Phys. Rev. B* **100**, 125141 (2019).
- [11] K.-E. Huhtinen and P. Törmä, Insulator-pseudogap crossover in the Lieb lattice, [arXiv:2007.05118](https://arxiv.org/abs/2007.05118).
- [12] N. Swain and M. Karmakar, Strain-induced superconductor-insulator transition on a Lieb lattice, *Phys. Rev. Res* **2**, 023136 (2020).
- [13] S. D. Huber and E. Altman, Bose condensation in flat bands, *Phys. Rev. B* **82**, 184502 (2010).
- [14] M. Tovmasyan, E. P. L. van Nieuwenburg, and S. D. Huber, Geometry induced pair condensation, *Phys. Rev. B* **88**, 220510(R) (2013).
- [15] V. I. Iglovikov, F. Hébert, B. Grémaud, G. G. Batrouni, and R. T. Scalettar, Superconducting transitions in flat-band systems, *Phys. Rev. B* **90**, 094506 (2014).
- [16] S. A. Parameswaran, R. Roy, and S. Sondhi, Fractional quantum Hall physics in topological flat bands, *C. R. Phys.* **14**, 816 (2013).
- [17] E. Bergholtz and Z. Liu, Topological Flat Band Models and Fractional Chern Insulators, *Int. J. Mod. Phys. B* **27**, 1330017 (2013).
- [18] S. Takayoshi, H. Katsura, N. Watanabe, and H. Aoki, Phase diagram and pair Tomonaga-Luttinger liquid in a Bose-Hubbard model with flat bands, *Phys. Rev. A* **88**, 063613 (2013).
- [19] B. Grémaud and G. G. Batrouni, Haldane phase on the sawtooth lattice: Edge states, entanglement spectrum, and the flat band, *Phys. Rev. B* **95**, 165131 (2017).
- [20] Y. Cao, V. Fatemi, A. Demir, S. Fang, S. Tomarken, J. Luo, J. Sanchez-Yamagishi, K. Watanabe, T. Taniguchi, E. Kaxiras, R. Ashoori, and P. Jarillo-Herrero, Correlated insulator behavior at half-filling in magic-angle graphene superlattices, *Nature (London)* **556**, 80 (2018).
- [21] Y. Cao, V. Fatemi, S. Fang, K. Watanabe, T. Taniguchi, E. Kaxiras, and P. Jarillo-Herrero, Un-conventional superconductivity in magic-angle graphene super-lattices, *Nature (London)* **556**, 43 (2018).
- [22] H. Guo, X. Zhu, S. Feng, and R. T. Scalettar, Pairing symmetry of interacting fermions on twisted bilayer graphene superlattice, *Phys. Rev. B* **97**, 235453 (2018).
- [23] A. Pinto, N. Frazao, D. Azevedo, and F. Moraes, Evidence for flat zero-energy bands in bilayer graphene with a periodic defect lattice, *Phys. E (Amsterdam, Neth.)* **119**, 113987 (2020).
- [24] J. M. Lee, C. Geng, J. W. Park, M. Oshikawa, S. S. Lee, H. W. Yeom, and G. Y. Cho, Stable Flatbands, Topology, and Superconductivity of Magic Honeycomb Networks, *Phys. Rev. Lett.* **124**, 137002 (2020).
- [25] C. Shen, Y. Chu, Q.-S. Wu, N. Li, S. Wang, Y. Zhao, J. Tang, J. Liu, J. Tian, K. Watanabe, T. Taniguchi, R. Yang, Z. Meng, D. Shi, O. Yazyev, and G. Zhan, Correlated states in twisted double bilayer graphene, *Nat. Phys.* **16**, 520 (2020).
- [26] D. Guzmán-Silva, C. Mejía-Cortés, M. A. Bandres, M. C. Rechtsman, S. Weimann, S. Nolte, M. Segev, A. Szameit, and R. A. Vicencio, Experimental observation of bulk and edge transport in photonic Lieb lattices, *New J. Phys.* **16**, 063061 (2014).
- [27] S. Mukherjee, A. Spracklen, D. Choudhury, N. Goldman, P. Öhberg, E. Andersson, and R. R. Thomson, Observation of a Localized Flat-Band State in a Photonic Lieb Lattice, *Phys. Rev. Lett.* **114**, 245504 (2015).
- [28] K. Noda, K. Inaba, and M. Yamashita, Flat-band ferromagnetism in the multilayer Lieb optical lattice, *Phys. Rev. A* **90**, 043624 (2014).
- [29] S. Xia, Y. Hu, D. Song, Y. Zong, L. Tang, and Z. Chen, Demonstration of flat-band image transmission in optically induced Lieb photonic lattices, *Opt. Lett.* **41**, 1435 (2016).
- [30] L. Santos, M. A. Baranov, J. I. Cirac, H.-U. Everts, H. Fehrmann, and M. Lewenstein, Atomic Quantum Gases in Kagome Lattices, *Phys. Rev. Lett.* **93**, 030601 (2004).
- [31] C. Wu, D. Bergman, L. Balents, and S. D. Sarma, Flat Bands and Wigner Crystallization in the Honeycomb Optical Lattice, *Phys. Rev. Lett.* **99**, 070401 (2007).
- [32] S. Li and S. Johnston, Quantum Monte Carlo study of lattice polarons in the two-dimensional three-orbital Su-Schrieffer-Heeger model, *NPJ Quantum Mater.* **5**, 40 (2020).

- [33] C. Feng, H. Guo, and R. T. Scalettar, Charge density waves on a half-filled decorated honeycomb lattice, *Phys. Rev. B* **101**, 205103 (2020).
- [34] T. Holstein, Studies of polaron motion: Part I. The molecular-crystal model, *Ann. Phys. (NY)* **8**, 325 (1959).
- [35] J. K. Freericks, M. Jarrell, and D. J. Scalapino, Holstein model in infinite dimensions, *Phys. Rev. B* **48**, 6302 (1993).
- [36] A. H. Romero, D. W. Brown, and K. Lindenberg, Effects of dimensionality and anisotropy on the Holstein polaron, *Phys. Rev. B* **60**, 14080 (1999).
- [37] L. C. Ku, S. A. Trugman, and J. Bonca, Dimensionality effects on the Holstein polaron, *Phys. Rev. B* **65**, 174306 (2002).
- [38] M. Hohenadler, H. G. Evertz, and W. von der Linden, Quantum Monte Carlo and variational approaches to the Holstein model, *Phys. Rev. B* **69**, 024301 (2004).
- [39] D. J. J. Marchand and M. Berciu, Effect of dispersive optical phonons on the behavior of a Holstein polaron, *Phys. Rev. B* **88**, 060301(R) (2013).
- [40] R. T. Scalettar, N. E. Bickers, and D. J. Scalapino, Competition of pairing and Peierls–charge-density-wave correlations in a two-dimensional electron-phonon model, *Phys. Rev. B* **40**, 197 (1989).
- [41] F. Marsiglio, Eliashberg theory of the critical temperature and isotope effect. Dependence on bandwidth, band-filling, and direct Coulomb repulsion, *J. Low Temp. Phys.* **87**, 659 (1992).
- [42] W. von der Linden, E. Berger, and P. Valášek, The Hubbard-Holstein model, *J. Low Temp. Phys.* **99**, 517 (1995).
- [43] A. S. Alexandrov, Breakdown of the Migdal-Eliashberg theory in the strong-coupling adiabatic regime, *Europhys. Lett.* **56**, 92 (2001).
- [44] A. V. Chubukov, A. Abanov, I. Esterlis, and S. A. Kivelson, Eliashberg theory of phonon-mediated superconductivity – when it is valid and how it breaks down, *Ann. Phys.* **417**, 168190 (2020).
- [45] P. M. Dee, J. Coulter, K. G. Kleiner, and S. Johnston, Relative importance of nonlinear electron-phonon coupling and vertex corrections in the Holstein model, *Commun. Phys.* **3**, 1 (2020).
- [46] R. M. Noack, D. J. Scalapino, and R. T. Scalettar, CDW and Pairing Susceptibilities in a Two-Dimensional Electron-Phonon Model, *Phys. Rev. Lett.* **66**, 778 (1991).
- [47] M. Vekić, R. M. Noack, and S. R. White, Charge-density waves versus superconductivity in the Holstein model with next-nearest-neighbor hopping, *Phys. Rev. B* **46**, 271 (1992).
- [48] O. Bradley and R. Scalettar, Superconductivity and charge density wave order in the 2DHolstein model, [arXiv:2011.11703](https://arxiv.org/abs/2011.11703).
- [49] R. T. Scalettar, D. J. Scalapino, R. L. Sugar, and D. Toussaint, Phase diagram of the half-filled 3D Hubbard model, *Phys. Rev. B* **39**, 4711 (1989).
- [50] M. Vekić and S. R. White, Gap formation in the density of states for the Holstein model, *Phys. Rev. B* **48**, 7643 (1993).
- [51] M. Weber and M. Hohenadler, Two-dimensional Holstein-Hubbard model: Critical temperature, Ising universality, and bipolaron liquid, *Phys. Rev. B* **98**, 085405 (2018).
- [52] N. C. Costa, M. V. Araújo, J. P. Lima, T. Paiva, R. R. dos Santos, and R. T. Scalettar, Compressible ferrimagnetism in the depleted periodic Anderson model, *Phys. Rev. B* **97**, 085123 (2018).
- [53] Y. X. Zhang, W. T. Chiu, N. C. Costa, G. G. Batrouni, and R. T. Scalettar, Charge Order in the Holstein Model on a Honeycomb Lattice, *Phys. Rev. Lett.* **122**, 077602 (2019).
- [54] B. Cohen-Stead, N. C. Costa, E. Khatami, and R. T. Scalettar, Effect of Strain on Charge Density Wave Order in the Holstein Model, *Phys. Rev. B* **100**, 045125 (2019).
- [55] C. Chen, X. Y. Xu, Z. Y. Meng, and M. Hohenadler, Charge-Density-Wave Transitions of Dirac Fermions Coupled to Phonons, *Phys. Rev. Lett.* **122**, 077601 (2019).
- [56] B. Xiao, N. C. Costa, E. Khatami, G. G. Batrouni, and R. T. Scalettar, Charge Density Wave and Superconductivity in the Disordered Holstein Model, [arXiv:1910.08703](https://arxiv.org/abs/1910.08703).
- [57] C. Chen, X. Y. Xu, J. Liu, G. Batrouni, R. Scalettar, and Z. Y. Meng, Symmetry-enforced self-learning Monte Carlo method applied to the Holstein model, *Phys. Rev. B* **98**, 041102(R) (2018).
- [58] S. Beyl, F. Goth, and F. F. Assaad, Revisiting the hybrid quantum Monte Carlo method for Hubbard and electron-phonon models, *Phys. Rev. B* **97**, 085144 (2018).
- [59] G. G. Batrouni and R. T. Scalettar, Langevin Simulations of a Long Range Electron Phonon Model, *Phys. Rev. B* **99**, 035114 (2019).
- [60] G. G. Batrouni and R. T. Scalettar, Quantum Monte Carlo with the Langevin Equation: Coupled Bose-Fermi Systems, *Commun. Comput. Phys.* **1290**, 012004 (2019).
- [61] Y. Zhang, C. Feng, G. G. Batrouni, and R. Scalettar (unpublished).
- [62] R. Blankenbecler, D. J. Scalapino, and R. L. Sugar, Monte Carlo calculations of coupled boson-fermion systems. I, *Phys. Rev. D* **24**, 2278 (1981).
- [63] S. Sorella, S. Baroni, R. Car, and M. Parinello, A Novel Technique for the Simulation of Interacting Fermion Systems, *Europhys. Lett.* **8**, 663 (1989).
- [64] N. C. Costa, T. Mendes-Santos, T. Paiva, R. R. dos Santos, and R. T. Scalettar, Ferromagnetism beyond Lieb’s theorem, *Phys. Rev. B* **94**, 155107 (2016).
- [65] W. S. Oliveira, N. C. Costa, J. Pimentel de Lima, and R. R. dos Santos, Classical and quantum percolation on the Lieb lattice (unpublished).
- [66] M. Bercx, J. S. Hofmann, F. F. Assaad, and T. C. Lang, Spontaneous particle-hole symmetry breaking of correlated fermions on the Lieb lattice, *Phys. Rev. B* **95**, 035108 (2017).
- [67] J. K. Freericks and D. J. Scalapino, Weak-coupling expansions for the attractive Holstein and Hubbard models, *Phys. Rev. B* **49**, 6368 (1994).